

Tilted optical lattices with defects as realizations of \mathcal{PT} symmetry in Bose-Einstein condensates

Manuel Kreibich, Jörg Main, Holger Cartarius, and Günter Wunner
Institut für Theoretische Physik 1, Universität Stuttgart, 70550 Stuttgart, Germany

A \mathcal{PT} -symmetric Bose-Einstein condensate can theoretically be described using a complex optical potential, however, the experimental realization of such an optical potential describing the coherent in- and outcoupling of particles is a nontrivial task. We propose an experiment for a quantum mechanical realization of a \mathcal{PT} -symmetric system, where the \mathcal{PT} -symmetric currents are implemented by an accelerating Bose-Einstein condensate in a titled optical lattice. A defect consisting of two wells at the same energy level then acts as a \mathcal{PT} -symmetric double-well if the tilt in the energy offsets of all further wells in the lattice is varied in time. We map the time-dependence of the amplitudes of a frozen Gaussian variational ansatz to a matrix model and increase the system size step by step starting with a six-well setup. In terms of this simple matrix model we derive conditions under which two wells of the Hermitian multi-well system behave *exactly* as the two wells of the \mathcal{PT} -symmetric system.

PACS numbers: 03.75.Kk, 03.65.Ge, 05.60.Gg, 11.30.Er

I. INTRODUCTION

One of the postulates of quantum mechanics tells us that an observable physical quantity is represented by a Hermitian operator. The postulate ensures that every eigenvalue of such an operator is real, and, since every result of a measurement corresponds to an eigenvalue of an operator, all measured quantities are real. One may now ask, if there is the possibility that, when dealing with a non-Hermitian Hamiltonian, an entirely or partially real eigenvalue spectrum occurs. The answer brings us to the notion of \mathcal{PT} symmetry.

\mathcal{PT} symmetry stands for the combined action of the operators parity reflection \mathcal{P} and time or motion reversal \mathcal{T} . A \mathcal{PT} -symmetric Hamiltonian does not necessarily have to be Hermitian. Nevertheless, BENDER and BOETTCHER found in their paper from 1998 [1] that there are parameter regimes in \mathcal{PT} -symmetric systems where the eigenvalue spectra are entirely real. The non-Hermiticity entering \mathcal{PT} -symmetric systems can be interpreted in that this is an effective description of an open quantum system with a situation of balanced gain and loss.

Due to a close analogy between the Schrödinger equation and the equations describing the propagation of light in structured wave guides, the theory of \mathcal{PT} symmetry was applied to these optical systems [2, 3]. Soon, the first \mathcal{PT} -symmetric optical systems could be realized [4, 5]. Other analogies with quantum mechanics could be used to create \mathcal{PT} -symmetric systems, including laser modes [6–8], electronics [9–11], and microwave cavities [12].

It was proposed [3] that a system similar to \mathcal{PT} -symmetric wave guides could be realized using a Bose-Einstein condensate (BEC) in a double-well potential, where in one well particles are injected, while from the other well particles are removed. However, as was already mentioned by the authors of Ref. [3] care must be taken with regard to the interaction in BECs since this

could modify or even destroy the \mathcal{PT} -symmetric properties. Nevertheless, BECs could provide an experimental realization of \mathcal{PT} symmetry in a genuine quantum system, which up to date is still missing.

In a schematic approach, the \mathcal{PT} -symmetric Bose-Hubbard model for two modes has been considered, and it could be shown that the mean-field limit is a good approximation even in the presence of a complex non-Hermitian potential [13–15]. In terms of the Gross-Pitaevskii equation (GPE) and a model δ -type potential it was confirmed that the nonlinear term entering the dynamical equation does not destroy the features of \mathcal{PT} -symmetry, rather these properties are maintained and even new prospects do appear [16, 17]. The extension of the model to a realistic external potential gives qualitatively the same results [18].

In all those investigations the \mathcal{PT} -symmetric potential was predetermined and no detailed mechanism was explained on how to actually realize \mathcal{PT} symmetry, which leaves some discomfort. As mentioned above, a non-Hermitian system is an effective description of an underlying Hermitian system, so when discussing in detail the realization of \mathcal{PT} -symmetry, this Hermitian system must be given.

It is the purpose of this work to demonstrate that a \mathcal{PT} -symmetric external potential for BECs can be realized with tilted optical lattices with a defect. The defect consisting of two potential wells at the same height, i. e., a discontinuity in the tilt, acts as a \mathcal{PT} -symmetric subsystem. The in- and outfluxes of the condensate's probability density can be modeled as imaginary \mathcal{PT} -symmetric contributions.

When such a system is explicitly given, an experimental realization of \mathcal{PT} symmetry in a BEC is possible. This is an important step in the research of \mathcal{PT} -symmetric BECs, since even when no future experiment is done according to the proposals of this work, the investigations performed in the above mentioned references are justified and the gap originating from the sketchiness

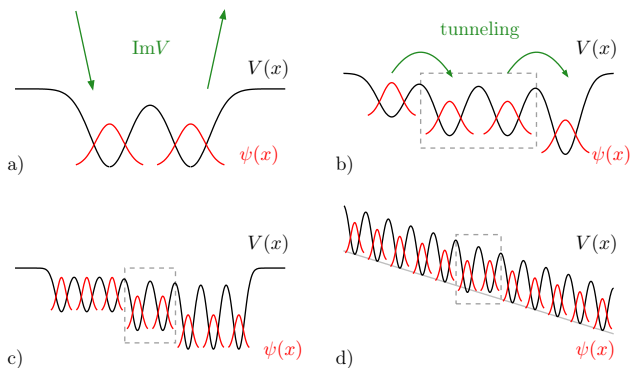


Figure 1. (Color online) (a) \mathcal{PT} -symmetric two-well system as discussed in Sec. II. The imaginary part of the external potential induces currents from the environment to the left well and from the right well to the environment. (b) By embedding the two-well system in two additional outer wells the tunneling currents may be used as an implementation of \mathcal{PT} -symmetry [19]. (c) With more outer wells the reservoir is larger, which can be advantageous. (d) In the limit of an infinite number of reservoir wells the system may be interpreted as the two-well system embedded in an optical lattice.

of the \mathcal{PT} -symmetric potential is closed.

There are several possibilities for a realization of \mathcal{PT} symmetry. In [20], the authors investigate the pointwise coupling of BECs with the possible exchange of particles at those points. In [21] another double-well system is suggested as a particle reservoir for the implementation of \mathcal{PT} -symmetry. However, in both references a coupling with no further specification is used. It is not clear, how such a coupling can be realized experimentally, which leaves some ambiguity in the possible realizations.

By contrast, we follow an alternative approach, which gives us a complete and realistic description of a possible realization. The basic idea on how to realize a \mathcal{PT} -symmetric two-well system as shown in Fig. 1(a) is sketched in Fig. 1(b): In this simple case the two-well system is embedded into a four-well system with two additional time-dependent wells. It has already been shown that the inner wells of this system can *exactly* behave as a \mathcal{PT} -symmetric double-well [19]. In this setup the occurrence of the tunneling currents from the outer wells to the inner ones may be used as a realization of \mathcal{PT} -symmetric gain and loss effects. Thus, the additional wells serve as particle reservoirs. Since there is a finite number of particles in the reservoirs \mathcal{PT} symmetry can only be realized for a finite time period. In principle an arbitrary number of particles could be filled in the reservoir. However, such a large difference of the number of particles between the embedded and reservoir wells could be a large challenge for an experiment, both for preparing and measuring the particle numbers.

Hence, in this paper we extend our previous investigations and use step by step more wells for a realization, see Fig. 1(c). In principle, an arbitrary number of wells, and

thus an arbitrary number of particles in the reservoir can be used, thus, maximizing the time that is available for realizing \mathcal{PT} symmetry. Using more wells consequently leads to the embedding of two wells into an optical lattice, Fig. 1(d), which allows us to use new tools and to obtain a new viewpoint on our method. The experimental realization of a multi-well potential that is necessary for our realization is possible with the method presented in [22].

This paper is organized as follows: In Sec. II we present the matrix model that is used throughout this work. In Sec. III we discuss how to realize \mathcal{PT} -symmetry within that model and derive conditions that must be fulfilled for the Hermitian system such that \mathcal{PT} -symmetry can be realized. In Sec. IV, these results are applied to six and more wells. Finally, in Sec. V we summarize our work and give an outlook to future work.

II. MATRIX MODELS

A BEC is described in the limit of large particle numbers by the GPE

$$i\hbar\frac{\partial}{\partial t}\psi(\mathbf{r}, t) = \left[-\frac{\hbar^2}{2m}\Delta + V(\mathbf{r}, t) + g|\psi(\mathbf{r}, t)|^2 \right] \psi(\mathbf{r}, t), \quad (1)$$

where $g = 4\pi\hbar^2 Na/m$ is the interaction strength with the s -wave scattering length a and the particle number N . The external potential V is time-dependent in this work and given by

$$V(\mathbf{r}, t) = \sum_{k=1}^{N_w} V^k(t) \exp\left(-\frac{2x^2}{w_x^2} - \frac{2y^2}{w_y^2} - \frac{2[z - s_z^k(t)]^2}{w_z^2}\right), \quad (2)$$

which is a superposition of Gaussian profiles for N_w wells. The quantity w_α designates the width in the direction α . The time-dependence is due to the depths $V^k(t) < 0$ of each well and the displacements along the z -direction $s_z^k(t)$. Such a potential can be created in an experiment with the method described in [22].

In [19] we presented a method to map the GPE (1) with the continuous potential (2) to a discrete, finite-dimensional system using a frozen Gaussian variational ansatz. This ansatz reads

$$\psi(\mathbf{r}, t) = \sum_{k=1}^{N_G} \psi^k(t) g^k(\mathbf{r}), \quad (3)$$

with the amplitudes ψ^k and the N_G Gaussian functions

$$g^k(\mathbf{r}) = \exp[-A_x^k x^2 - A_y^k y^2 - A_z^k (z - q_z^k)^2]. \quad (4)$$

Throughout this paper we assume that $N_G = N_w$, i. e. we use one Gaussian function located in one well, $q_z^k \approx s_z^k$. After integrating out the spatial dependencies and

performing a symmetric orthogonalization [23] we arrive at

$$i\hbar\dot{\psi} = \mathbf{H}\psi \quad (5)$$

with the Hamiltonian in nearest-neighbor approximation

$$H_{kl}(t) = \begin{cases} E_k(t) + g_k |\psi_k(t)|^2, & \text{for } k = l, \\ -J_{kl}(t), & \text{for } |k - l| = 1, \\ 0, & \text{otherwise.} \end{cases} \quad (6)$$

The time-dependencies of the parameters of the potential (2) are mapped to time-dependencies of the onsite energies $E_k(t)$ and the tunneling elements $J_{kl}(t)$. The relation between the parameters V^k , s_z^k on one hand and E_k , J_{kl} on the other hand can be found in [19].

As an example, for a \mathcal{PT} -symmetric two-well system $N_w = 2$ with $\text{Re } V^1 = \text{Re } V^2$ and $\text{Im } V^1 = -\text{Im } V^2$ we obtain

$$\mathbf{H} = \begin{pmatrix} i\Gamma + g |\psi_1|^2 & -J_{12} \\ -J_{12} & -i\Gamma + g |\psi_2|^2 \end{pmatrix}, \quad (7)$$

where for convenience the energy has been moved such that the onsite energies are zero. A detailed and comprehensive analysis of this system, which is sketched in Fig. 1(a), can be found in [24].

III. REALIZING \mathcal{PT} SYMMETRY

A. Preliminary calculations

Before going on, we present some calculations that are necessary for later considerations in terms of the few-mode model. For a discrete system with N_w wells, a state is described by the vector $\psi \in \mathbb{C}^{N_w}$. This time-dependent vector is a solution of the time-dependent discrete GPE (5) with the Hamiltonian (6). The modulus squared of vector entry k is interpreted as proportional to the number of particles in well k , that is $n_k = |\psi_k|^2$. When ψ is normalized to unity for N particles, then the number of particles in well k is $N_k = Nn_k$. The time derivative of n_k can be calculated using the GPE, which yields

$$\frac{dn_k}{dt} = j_{k-1,k} - j_{k,k+1}, \quad (8)$$

where we used $H_{kl} = H_{lk}^*$. The current from well k to well l with $|k - l| = 1$, j_{kl} , is given by

$$j_{kl} = \frac{i}{\hbar} J_{kl} (\psi_k \psi_l^* - \psi_k^* \psi_l) = -j_{lk}. \quad (9)$$

For later convenience we define the ‘‘modified’’ current by

$$\tilde{j}_{kl} = i(\psi_k \psi_l^* - \psi_k^* \psi_l) = j_{kl} \frac{\hbar}{J_{kl}}, \quad (10)$$

which is just the dimensionless current. The current j_{kl} is only defined for adjacent wells, whereas the modified current \tilde{j}_{kl} can be used for arbitrary distances between the wells. The time derivative of the modified current can be calculated by similar means, this gives

$$\hbar \frac{d\tilde{j}_{kl}}{dt} = (E_k + g_k n_k - E_l - g_l n_l) C_{kl} - \zeta_{kl}, \quad (11)$$

where we defined the quantity

$$C_{kl} = \psi_k \psi_l^* + \psi_k^* \psi_l = C_{lk} \quad (12)$$

and the abbreviation

$$\zeta_{kl} = J_{k-1,k} C_{k-1,l} + J_{k,k+1} C_{k+1,l} - J_{l-1,l} C_{k,l-1} - J_{l,l+1} C_{k,l+1}. \quad (13)$$

Finally, the time derivative of C_{kl} is given by

$$\hbar \frac{dC_{kl}}{dt} = (E_l + g_l n_l - E_k - g_k n_k) \tilde{j}_{kl} + \eta_{kl} \quad (14)$$

with

$$\eta_{kl} = J_{k-1,k} \tilde{j}_{k-1,l} + J_{k,k+1} \tilde{j}_{k+1,l} - J_{l-1,l} \tilde{j}_{k,l-1} - J_{l,l+1} \tilde{j}_{k,l+1}. \quad (15)$$

B. Derivations of conditions

The nonlinear \mathcal{PT} -symmetric two-mode model is given by the Hamiltonian (7). The time derivative of the number of particles per well, $n_k = |\psi_k|^2$, leads to the closed set of coupled real differential equations

$$\frac{dn_1}{dt} = -j_{12} + 2\Gamma n_1 / \hbar, \quad (16a)$$

$$\frac{dn_2}{dt} = j_{12} - 2\Gamma n_2 / \hbar, \quad (16b)$$

$$\hbar \frac{d\tilde{j}_{12}}{dt} = 2J_{12}(n_1 - n_2) + g(n_1 - n_2)C_{12}, \quad (16c)$$

$$\hbar \frac{dC_{12}}{dt} = -g(n_1 - n_2)\tilde{j}_{12}. \quad (16d)$$

When we want to realize the system using a larger Hermitian system, we have to make sure that two wells of the larger system behave exactly as the two wells of the \mathcal{PT} -symmetric two-mode model, that means the time derivatives of the observables must be equivalent to Eqs. (16).

We now think of embedding the two wells of the \mathcal{PT} -symmetric system in a larger system with an arbitrary number of wells. The two wells that shall behave like the \mathcal{PT} -symmetric two-mode model (which are called *embedded wells* from now on) have the indices m and $m + 1$. The Hamiltonian for the multi-mode model is given in nearest-neighbor approximation by Eq. (6). The onsite energies E_k and the tunneling elements $J_{kl} = J_{lk}$ are in general time-dependent and real despite of the

energies for the embedded wells, which are given by $E_m = E_{m+1} = 0$, and the tunneling element $J_{m,m+1}$ that is time-independent.

We continue by calculating the time derivatives of the observables for the embedded wells m and $m+1$ of the multi-mode model (6), which yields

$$\frac{dn_m}{dt} = j_{m-1,m} - j_{m,m+1}, \quad (17a)$$

$$\frac{dn_{m+1}}{dt} = j_{m,m+1} - j_{m+1,m+2}, \quad (17b)$$

$$\begin{aligned} \hbar \frac{d\tilde{j}_{m,m+1}}{dt} &= 2J_{m,m+1}(n_m - n_{m+1}) \\ &+ (g_m n_m - g_{m+1} n_{m+1}) C_{m,m+1} \\ &- J_{m-1,m} C_{m-1,m+1} + J_{m+1,m+2} C_{m,m+2}, \end{aligned} \quad (17c)$$

$$\begin{aligned} \hbar \frac{dC_{m,m+1}}{dt} &= -(g_m n_m - g_{m+1} n_{m+1}) \tilde{j}_{m,m+1} \\ &+ J_{m-1,m} \tilde{j}_{m-1,m+1} - J_{m+1,m+2} \tilde{j}_{m,m+2}. \end{aligned} \quad (17d)$$

If we now identify the wells 1 and 2 of the \mathcal{PT} -symmetric two-mode model (16) with wells m and $m+1$ of the general multi-mode model (17), we find that the nonlinear interaction strengths must be equal for the multi-mode model, i. e. $g_m = g_{m+1} = g$. Then, we obtain conditions that must be fulfilled such that the embedded wells of the multi-mode model behave exactly as the two wells of the \mathcal{PT} -symmetric system. These conditions are

$$j_{m-1,m} = 2\Gamma n_m / \hbar, \quad (18a)$$

$$j_{m+1,m+2} = 2\Gamma n_{m+1} / \hbar, \quad (18b)$$

$$J_{m-1,m} C_{m-1,m+1} = J_{m+1,m+2} C_{m,m+2}, \quad (18c)$$

$$J_{m-1,m} \tilde{j}_{m-1,m+1} = J_{m+1,m+2} \tilde{j}_{m,m+2}. \quad (18d)$$

This is the first central result on our way to realize \mathcal{PT} symmetry: If these conditions can be fulfilled for a finite time period, then in this time we are able to realize \mathcal{PT} symmetry. It remains to show that these conditions can indeed be fulfilled by giving the matrix elements of the multi-mode model (6), and further that this choice can be established for a finite time.

Before we move on, we discuss the conditions (18) considering the number of independent constraints. With four independent equations we must use four matrix elements to fulfill these equations. It can be shown that only three conditions are independent and the fourth can be deduced [19]. Thus, we treat Eqs. (18a)–(18c) as independent.

C. Solution for matrix elements

So far, we have derived conditions under which the embedded wells in a Hermitian multi-well model behave exactly as the \mathcal{PT} -symmetric two-mode model. Condition (18c) can simply be fulfilled by setting the tunneling

elements

$$J_{m-1,m} = dC_{m,m+2}, \quad J_{m+1,m+2} = dC_{m-1,m+1}, \quad (19)$$

with an arbitrary time-dependent function $d = d(t)$. There are two conditions remaining, namely

$$\hbar j_{m-1,m} = J_{m-1,m} \tilde{j}_{m-1,m} \stackrel{!}{=} 2\Gamma n_m, \quad (20a)$$

$$\hbar j_{m+1,m+2} = J_{m+1,m+2} \tilde{j}_{m+1,m+2} \stackrel{!}{=} 2\Gamma n_{m+1}. \quad (20b)$$

Since both tunneling elements are determined by Eqs. (19), there are no free parameters left to fulfill Eqs. (20) at a given time.

However, there is a possibility to ensure that Eqs. (20) are fulfilled. To see this, we take the time derivative of these equations, which gives

$$\begin{aligned} 2 \frac{d\Gamma}{dt} n_m + 2\Gamma \frac{dn_m}{dt} &= \frac{dJ_{m-1,m}}{dt} \tilde{j}_{m-1,m} \\ &+ J_{m-1,m} \frac{d\tilde{j}_{m-1,m}}{dt}, \end{aligned} \quad (21a)$$

$$\begin{aligned} 2 \frac{d\Gamma}{dt} n_{m+1} + 2\Gamma \frac{dn_{m+1}}{dt} &= \frac{dJ_{m+1,m+2}}{dt} \tilde{j}_{m+1,m+2} \\ &+ J_{m+1,m+2} \frac{d\tilde{j}_{m+1,m+2}}{dt}, \end{aligned} \quad (21b)$$

where we allow for a time-dependent value of Γ . For further evaluation we need to calculate the time derivatives of the quantities \tilde{j}_{kl} , which are given in Eq. (11).

For the time derivatives of the tunneling elements we need the time derivative of d in Eq. (19), which is not determined at this point. We assume that \dot{d} contains terms that are at most linear in the energies E_{m-1} and E_{m+2} . As it turns out later, this is indeed the case for all choices of the time-dependent function $d(t)$ in this work. We write

$$\hbar \dot{d} = D_{m-1} E_{m-1} + D_{m+2} E_{m+2} + D, \quad (22)$$

where D contains all other quantities and all D -quantities are independent of E_{m-1} and E_{m+2} .

When inserting all calculated expressions, Eqs. (21) give a linear system of equations for the onsite energies E_{m-1} and E_{m+2} ,

$$\begin{pmatrix} M_{m-1,m-1} & M_{m-1,m+2} \\ M_{m+2,m+1} & M_{m+2,m+2} \end{pmatrix} \begin{pmatrix} E_{m-1} \\ E_{m+2} \end{pmatrix} = \begin{pmatrix} v_{m-1} \\ v_{m+2} \end{pmatrix}, \quad (23)$$

with the matrix entries

$$M_{m-1,m-1} = C_{m,m+2} (D_{m-1} \tilde{j}_{m-1,m} + dC_{m-1,m}), \quad (24a)$$

$$M_{m-1,m+2} = \tilde{j}_{m-1,m} (D_{m+2} C_{m,m+2} + d\tilde{j}_{m,m+2}), \quad (24b)$$

$$\begin{aligned} M_{m+2,m-1} &= D_{m-1} C_{m-1,m+1} \tilde{j}_{m+1,m+2} \\ &- d\tilde{j}_{m-1,m+1} \tilde{j}_{m+1,m+2}, \end{aligned} \quad (24c)$$

$$\begin{aligned} M_{m+2,m+2} &= D_{m+2} C_{m-1,m+1} \tilde{j}_{m+1,m+2} \\ &- dC_{m-1,m+1} C_{m+1,m+2}, \end{aligned} \quad (24d)$$

and vector entries

$$\begin{aligned}
v_{m-1} = & 2\hbar\dot{\Gamma}n_m - 2\hbar\Gamma j_{m,m+1} + 4\Gamma^2 n_m \\
& - D\tilde{j}_{m-1,m}C_{m,m+2} - d\tilde{j}_{m-1,m}\eta_{m,m+2} \\
& - d\tilde{j}_{m-1,m}\tilde{j}_{m,m+2}(g_{m+2}n_{m+2} - g_m n_m) \\
& - dC_{m-1,m}C_{m,m+2}(g_{m-1}n_{m-1} - g_m n_m) \\
& + dC_{m,m+2}\zeta_{m+1,m}, \tag{25a}
\end{aligned}$$

$$\begin{aligned}
v_{m+2} = & 2\hbar\dot{\Gamma}n_{m+1} + 2\hbar\Gamma j_{m,m+1} - 4\Gamma^2 n_{m+1} \\
& - DC_{m-1,m+1}\tilde{j}_{m+1,m+2} - d\tilde{j}_{m+1,m+2}\eta_{m-1,m+1} \\
& - d\tilde{j}_{m-1,m+1}\tilde{j}_{m+1,m+2}(g_{m+1}n_{m+1} - g_{m-1}n_{m-1}) \\
& - dC_{m-1,m+1}C_{m+1,m+2}(g_{m+1}n_{m+1} - g_{m+2}n_{m+2}) \\
& + dC_{m-1,m+1}\zeta_{m+1,m+2}. \tag{25b}
\end{aligned}$$

Note the appearance of the tunneling rates $J_{m-2,m-1}$ and $J_{m+2,m+3}$. For the four-well system, these quantities do not appear in the Hamiltonian. In this case, they have to be set to zero in the equations. If there are more than four wells, the tunneling rates can be arbitrary and time-dependent. Whereas Eqs. (19) can always be fulfilled, for the linear system of equations (23) the determinant of the coefficient matrix must not vanish. This indicates that \mathcal{PT} symmetry cannot be realized for all conditions and for an arbitrary long time period. In Sec. III D we discuss cases in which the determinant vanishes.

What have we gained by considering the time derivatives of Eqs. (20)? We have seen that there are no free parameters left to fulfill these equations. However, we now have conditions for the onsite energies E_{m-1} and E_{m+2} such that the time derivatives of both sides of each equation are equal. If we make sure that Eqs. (20) are fulfilled for the initial time and the onsite energies are chosen according to Eqs. (23), then the conditions are fulfilled for every time. We set the four matrix elements of the Hamiltonian (6) $J_{m-1,m}$, $J_{m+1,m+2}$, E_{m-1} , E_{m+2} , and have one degree of freedom with the function d , then the three independent conditions (18a)–(18c) are fulfilled and we have a realization of \mathcal{PT} -symmetry.

D. Choices for the function d

Before investigating specific scenarios of realizing \mathcal{PT} symmetry, we discuss two possibilities of choosing the time-dependent function d . We want to point out that a different choice of d does not change the dynamics of the observables, rather it changes the values of the matrix elements $J_{m-1,m}$, $J_{m+1,m+2}$, E_{m-1} , and E_{m+2} .

1. Constant d

The most simple possibility is a time-independent d , i. e. $\dot{d} = 0$, from which it follows that $D_{m-1} = D_{m+2} = D = 0$. Then, the determinant of the coefficient matrix \mathbf{M} in Eq. (23) can be expressed with the analytical results

of [19] as

$$\det \mathbf{M} = \pm 16d^2 n_{m-1} n_m n_{m+1} n_{m+2} \sqrt{(1-\alpha)^2 - \beta^2} \tag{26}$$

with the plus or minus sign depending on the initial conditions and

$$\alpha = (\beta + \gamma)\gamma, \quad \beta = \frac{\Gamma}{d\sqrt{n_{m-1}n_{m+2}}}, \quad \gamma = \frac{\tilde{j}_{m,m+1}}{2\sqrt{n_m n_{m+1}}}. \tag{27}$$

When either one of the reservoir or embedded wells is empty, the conditions cannot be fulfilled. Additionally, the term in the square root in Eq. (26) can be zero, which can be rewritten to

$$\beta = -\gamma \pm 1. \tag{28}$$

When the number of particles in the reservoir wells, i. e. n_{m-1} and n_{m+2} , is large enough, the linear system of equations can be solved. However, before these wells get empty, there is the possibility that there are no solutions for the onsite energies anymore. The time-independent parameter d can then be changed to another (larger) value in a new simulation, which does modify the resulting matrix elements $J_{m-1,m}$, $J_{m+1,m+2}$, E_{m-1} , and E_{m+2} .

2. Compensating the time-dependence of the tunneling elements

Suppose that for the initial time the tunneling elements $J_{m-1,m}$ and $J_{m+1,m+2}$ are given by the trapping geometry. With Eq. (19) these tunneling elements depend on time, which can be difficult to realize in a given geometry. When we want $J_{m-1,m}$ to be fixed to the initial value $J_{m-1,m}^{(0)}$, then we must require

$$J_{m-1,m} = dC_{m,m+2} \stackrel{!}{=} J_{m-1,m}^{(0)} \Leftrightarrow d = \frac{J_{m-1,m}^{(0)}}{C_{m,m+2}}. \tag{29}$$

Similar, if we want $J_{m+1,m+2}$ to be fixed, d must be chosen to

$$d = \frac{J_{m+1,m+2}^{(0)}}{C_{m-1,m+1}}. \tag{30}$$

Both conditions cannot be fulfilled at the same time, however if we demand the actual value of d to be the average of both possibilities, we have an ‘‘average’’ fulfillment. The time-dependent value of d is then

$$d = \frac{J_{m-1,m}^{(0)}}{2C_{m,m+2}} + \frac{J_{m+1,m+2}^{(0)}}{2C_{m-1,m+1}}. \tag{31}$$

To calculate the onsite energies, we need the time derivative of d . We get for the parameters in Eq. (22)

$$D_{m-1} = \frac{J_{m+1,m+2}^{(0)}}{2C_{m-1,m+1}^2} \tilde{j}_{m-1,m+1}, \quad (32a)$$

$$D_{m+2} = -\frac{J_{m-1,m}^{(0)}}{2C_{m,m+2}^2} \tilde{j}_{m,m+2}, \quad (32b)$$

and

$$\begin{aligned} D = & -\frac{J_{m-1,m}^{(0)}}{2C_{m,m+2}^2} (g_{m+2}n_{m+2} - g_m n_m) \tilde{j}_{m,m+2} \\ & -\frac{J_{m+1,m+2}^{(0)}}{2C_{m-1,m+1}^2} (g_{m+1}n_{m+1} - g_{m-1}n_{m-1}) \tilde{j}_{m-1,m+1} \\ & -\frac{J_{m-1,m}^{(0)}}{2C_{m,m+2}^2} \eta_{m,m+2} - \frac{J_{m+1,m+2}^{(0)}}{2C_{m-1,m+1}^2} \eta_{m-1,m+1}. \end{aligned} \quad (32c)$$

As with the case of a constant d we evaluate the determinant of the coefficient matrix \mathbf{M} in Eq. (23) to investigate for which time period the system of equations can be solved. The determinant can be evaluated analytically, and after a lengthy calculation we obtain

$$\det \mathbf{M} = 8n_{m-1}n_m n_{m+1}n_{m+2}d^2 \times \left(\pm \sqrt{(1-\alpha)^2 - \beta^2} + \gamma^2 - 1 \right). \quad (33)$$

Compared to the case of constant d the additional term $\gamma^2 - 1$ appears in the bracket. As before, when one of the wells is empty the determinant is zero. For additional roots we have to consider the term in the bracket. This yields the solutions $\beta = 0$ and $\beta = -2\gamma$ with the plus sign in Eq. (33), otherwise there are no solutions. If we can make sure that for a certain realization the minus sign is chosen in Eq. (33) then the linear system of equations can be solved as long as the embedded and reservoir wells are not empty, which is an advantage compared to the case of constant d .

E. Choices for other matrix elements in the multi-mode model

With the previous investigations we fixed the matrix elements of the Hamiltonian (6) $J_{m-1,m}$, $J_{m+1,m+2}$, E_{m-1} , and E_{m+2} of the multi-mode model. For the minimal four-mode model [19, 25], all matrix elements are determined and no freedom is left, despite the function d . When using more than four wells, the additional tunneling elements and onsite energies are not fixed by the conditions (18a)–(18c) and may be chosen arbitrarily. In this section we give the three possibilities that we use in this work. For all choices we assume that the tunneling elements are time-independent besides $J_{m-1,m}$ and $J_{m+1,m+2}$, which are determined by Eqs. (19).

1. Leveling out onsite energies

One of the simplest possibilities is to choose the energies of the wells to the left of the embedded wells equal to E_{m-1} , and the energies of the wells to the right equal to E_{m+2} , both of which are determined by Eqs. (23), that means

$$E_k = \begin{cases} E_{m-1}, & \text{for } k < m-1, \\ E_{m+2}, & \text{for } k > m+2. \end{cases} \quad (34)$$

With this method one effectively enlarges the particle reservoir, which allows for increasing the time where \mathcal{PT} symmetry is available. This choice is sketched in Fig. 1(c).

2. Requiring specific currents

For wells $m-1$ and $m+2$ we have chosen the energies such that the currents $j_{m-1,m}$ and $j_{m+1,m+2}$ obtain a given value. This should also be possible for the other currents. We assume target values of the currents $j_{k,k+1}^{\text{tar}}$ for $1 \leq k \leq m-2$ and $m+2 \leq k \leq N_w - 1$ that may be time-dependent. We take the time derivatives of these currents, which yields with Eq. (11)

$$E_k = \frac{\hbar^2}{J_{k,k+1}C_{k,k+1}} \frac{dj_{k,k+1}^{\text{tar}}}{dt} + \frac{\zeta_{k,k+1}}{C_{k,k+1}} + E_{k+1} - g_k n_k + g_{k+1} n_{k+1}, \quad (35)$$

where we consider the case $1 \leq k \leq m-2$ and assume that E_{k+1} is determined. Beginning with $k = m-2$ we can consecutively calculate the onsite energies for the wells to the left of the embedded wells down to the well $k = 1$. By similar means we get

$$E_{k+1} = -\frac{\hbar^2}{J_{k,k+1}C_{k,k+1}} \frac{dj_{k,k+1}^{\text{tar}}}{dt} - \frac{\zeta_{k,k+1}}{C_{k,k+1}} + E_k + g_k n_k - g_{k+1} n_{k+1}. \quad (36)$$

for the wells to the right. Note that, as with the onsite energies E_{m-1} and E_{m+2} , the initial wave function ψ must correspond to the target currents, since we only consider the time derivative to derive the onsite energies.

3. Optical lattice with Stark potential

When E_{m-1} and E_{m+2} are given by Eqs. (23) we can choose the other onsite energies such that they form an optical lattice with a linear Stark potential with

$$E_k = \begin{cases} 0, & \text{for } k = m, m+1, \\ [k - (m+1/2)] \Delta E + E^{(0)}, & \text{otherwise,} \end{cases} \quad (37)$$

where we have chosen the middle of the embedded wells as the center, which explains the term $m + 1/2$, see Fig. 1(d). With E_{m-1} and E_{m+2} the slope ΔE and offset $E^{(0)}$ can be determined, which yields

$$\Delta E = \frac{1}{3} (E_{m+2} - E_{m-1}), \quad (38a)$$

$$E^{(0)} = \frac{1}{2} (E_{m-1} + E_{m+2}). \quad (38b)$$

Note that $E_m = E_{m-1} = 0$ are not determined by the linear Stark potential so that they can be interpreted as a perturbation. This possibility should allow for an easy experimental realization as an optical lattice with a linear Stark potential is an approved technique used in many experiments.

F. Fourier ansatz for an optical lattice

The matrix model given by the Hamiltonian (6) can be solved by the usual methods: Either one can diagonalize the Hamiltonian matrix analytically or by using numerical methods. However, for the special case of an optical lattice with an infinite number of wells, where the onsite energies are the same for each well, there are specific solution methods available. A simple quantum mechanical model for an optical lattice is the discrete Schrödinger equation with an infinite number of wells, where the Hamiltonian is defined as

$$H_{kl} = \begin{cases} -J, & \text{for } |k - l| = 1, \\ 0, & \text{else.} \end{cases} \quad (39)$$

The onsite energies are set to zero, and the tunneling elements are assumed to be the same for each well barrier. The eigenstates are given by

$$\psi_{q,n} = A \exp(iqn) \quad (40)$$

with lattice index n and quantum number q , with the eigenvalues

$$E(q) = -2J \cos q, \quad (41)$$

where $q \in [-\pi, \pi]$. With these results it is clear that our model features only one band as opposed to a more extended model [26], where the continuous Schrödinger equation is solved. When we include an interaction in our model via the mean-field approximation with non-vanishing interaction strengths g_k the eigenstates (40) are still solutions. However, new solutions appear that may break the translational symmetry of the model, and the solutions (40) may become unstable with respect to small perturbations, both of which we will not consider in this work.

A general time-dependent solution of the linear Schrödinger equation has the form

$$\psi_n(t) = \int_{-\pi}^{\pi} dq f(q) \exp[i(qn - E(q)t/\hbar)]. \quad (42)$$

An analytical solution of this equation is not available. However, there is an important approximation called the *semiclassical approximation* that is valid, when the amplitude $f(q)$ is sharply centered around a value q_0 . In this case the wave function reads [26]

$$\begin{aligned} \psi_n(t) = & \exp[i(q_0 n - E(q_0)t/\hbar)] \\ & \times \int_{-\pi}^{\pi} dq f(q) \exp[i(n - v_g(q_0)t)(q - q_0)] \\ & \times \exp\left[-i\hbar t (q - q_0)^2 / 2m_{\text{eff}}(q_0)\right] \end{aligned} \quad (43)$$

with

$$v_g(q_0) = E'(q_0)/\hbar, \quad m_{\text{eff}}(q_0) = \hbar^2/E''(q_0) \quad (44)$$

the *group velocity* and *effective mass*, respectively. The wave packet moves with group velocity v_g and disperses analogously to a free wave packet (without a potential) describing a particle with mass m_{eff} . Connected with the propagating wave packet is a current: When a wave packet moves, for instance, to the right and a single well is considered, there is a particle flow to this well out of the left side and a flow from this well to the right side.

With the Hamiltonian given by Eq. (39) the movement of a wave packet cannot be changed. We therefore introduce a linear Stark potential, where the onsite energies are given by $E_k = \Delta E k$. When ΔE is constant and the semiclassical approximation is used, the center of the momentum distribution gets time-dependent according to $q_0(t) = q_0(0) + \Delta E t/\hbar$ [26]. The quasi-momentum q_0 has a linear time-dependence, but when inserted into the group velocity, this leads to

$$v_g(q_0) = E'(q_0)/\hbar = \frac{2J}{\hbar} \sin\left[q_0(0) + \frac{\Delta E t}{\hbar}\right]. \quad (45)$$

The group velocity oscillates in time, and with it the position of the wave packet according to $\dot{n}_0 = v_g(q_0)$. This is an occurrence of the famous *Bloch oscillation* due to a constant force in a periodic potential. This model can be extended to a time-dependent force ΔE by

$$\dot{q}_0(t) = \Delta E(t)/\hbar, \quad \dot{n}_0(t) = v_g(q_0(t)). \quad (46)$$

Now the time derivative of the pseudo-momentum q_0 is proportional to the force ΔE , which explains the notion “semiclassical approximation”. The term in Eq. (43) containing the effective mass must also be generalized according to

$$\frac{t}{m_{\text{eff}}(q_0)} \rightarrow \int_0^t dt' \frac{1}{m_{\text{eff}}(q_0(t'))} \equiv \frac{t}{\bar{m}_{\text{eff}}(t)}. \quad (47)$$

When the sharp momentum peak of $f(q)$ in Eq. (43) does not come close to the border of the Brillouin zone, we can extend the interval of the integral in Eq. (43) to $[-\infty, \infty]$ and we are able to explicitly calculate the wave function. We make use of this possibility when discussing the realization of \mathcal{PT} -symmetry in terms of optical lattices in Sec. IV C.

IV. RESULTS OF SIMULATIONS

In Sec. III we developed the central idea to realize \mathcal{PT} symmetry by embedding a \mathcal{PT} -symmetric two-well system into a larger Hermitian system. It is the purpose of this section to apply the theoretical results and to investigate numerically actual realizations. The most simple system with which we can realize a \mathcal{PT} -symmetric system contains at each side one additional reservoir well, which gives in total a four-well system. Results for this minimal four-well system are presented in our Rapid Communication [25] and more comprehensively in [19]. We showed that with a four-well system we can realize \mathcal{PT} -symmetry for suitable long times and that by choosing the reservoir wells larger and larger we can extend the time that is available for realizing \mathcal{PT} -symmetry. This, however, is in an experimental setup limited for two reasons. At first, a large difference in the particle population between the inner and outer wells can be difficult to measure in an experiment. In addition, a large population in the reservoir wells can make the onsite energies extremely large, which would be another difficulty in an experimental setup.

For this reasons we continue the investigations started in [25] by choosing more than two reservoir wells and consequently increasing the number of wells which leads us to the discussion of \mathcal{PT} -symmetric currents in optical lattices with a linear Stark potential. Here, we give only a few example calculations. More can be found in [27].

A. Six-mode model

1. Leveling out onsite energies

We start with the six-mode model with one additional reservoir well on each side compared to the four-mode model. This is the most simple extension of the four-mode system with a symmetric number of wells on each side of the embedded wells. It effectively enlarges the reservoir, since the reservoir wells directly coupled to the embedded wells can now be fed by the outer wells and thus the time that is available for realizing \mathcal{PT} symmetry is extended. As a first example we consider the case where the additional wells are chosen to be at the same energy level as the wells directly coupled to the embedded wells, so called *leveled out* energies. For the six-mode model this implies

$$E_1 = E_2, \quad E_5 = E_6, \quad (48)$$

where wells $m = 3$ and $m + 1 = 4$ are the embedded wells. All matrix elements are now fixed, solely the initial wave functions in wells 1 and 6 are arbitrary and thus the initial populations and currents to the adjacent wells. A somewhat naive approach to choose arbitrary values of the parameters of the initial wave function is a possibility, but this results in large oscillations between the reservoir wells, which is a valid, but not a suitable realization for an experiment.

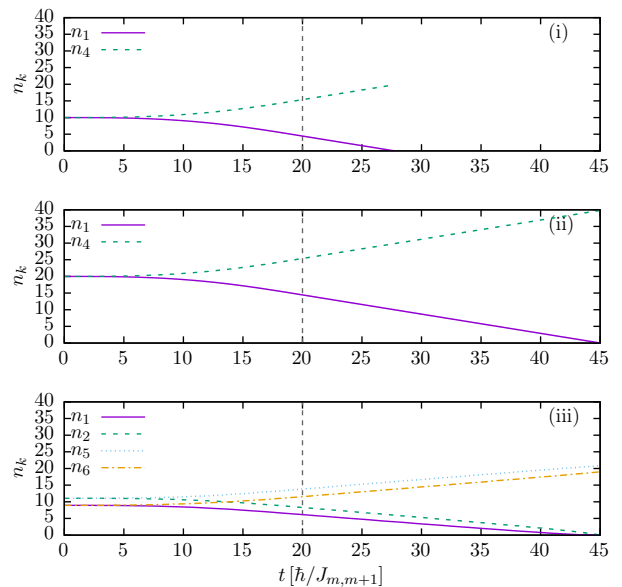


Figure 2. (Color online) (i) Population of the outer wells for the four-mode model, where an adiabatic current ramp is simulated with a final time of $t_{\text{tar}} = 20\hbar/J_{m,m+1}$. (ii) The time that is available for realizing \mathcal{PT} symmetry should be extended. On the one hand one can simply increase the initial number of particles in the reservoir wells. (iii) On the other hand the six-mode model can be used to effectively enlarge the reservoir. Now the difference of the particle numbers between the embedded and reservoir wells is smaller, which could help to measure the well population in an experiment. The nearly constant population of the embedded wells $n_m(t) = n_{m+1}(t) \approx 0.5$ is not shown.

Hence, the initial conditions must be chosen carefully. A natural solution is the use of the adiabatic current ramp [19], where the initial condition is the ground state of a Hermitian system and the \mathcal{PT} -parameter is time-dependently varied as

$$\Gamma(t) = \begin{cases} 0, & \text{for } t < 0, \\ \Gamma_{\text{tar}} [1 - \cos(\pi t/t_{\text{tar}})]/2 & \text{for } 0 \leq t \leq t_{\text{tar}}, \\ \Gamma_{\text{tar}}, & \text{for } t > t_{\text{tar}} \end{cases} \quad (49)$$

with target parameter Γ_{tar} reached at $t = t_{\text{tar}}$. To investigate the use of the six-mode model, we simulate three different scenarios that allow us a comparison. All cases have the adiabatic current ramp with a target value of $\Gamma_{\text{tar}}/J_{m,m+1} = 0.5$ in common, which is reached at a target time of $t_{\text{tar}} = 20\hbar/J_{m,m+1}$. The initial population for the embedded wells is always $n_m = n_{m+1} = 0.5$. (i) For the first run, we use the four-mode model with an initial population for the reservoir wells of $n_1 = n_4 = 10$. (ii) Still with the four-mode model, for the second simulation the particle number in the reservoir wells is doubled to $n_1 = n_4 = 20$. (iii) For the third scenario we use the six-mode model, where the onsite energies are chosen such that for the initial time we have $n_1 + n_2 = n_5 + n_6 = 20$, giving the same number of reservoir particles as in the

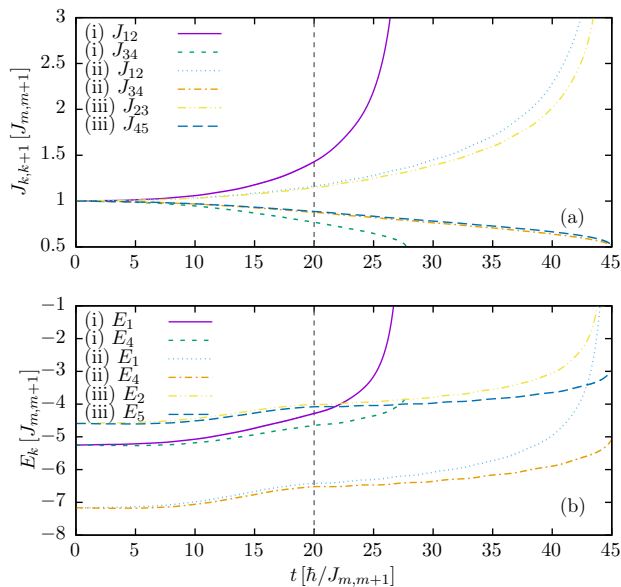


Figure 3. (Color online) (a) Tunneling elements $J_{m-1,m}$, $J_{m+1,m+2}$ and (b) onsite energies E_m , E_{m+1} for the scenarios (i)–(iii) discussed in Fig. 2. Comparing (ii) and (iii), for the tunneling elements there is not much difference. The onsite energies, however, differ by some amount. The magnitude for the six-mode model is smaller, which could be an advantage in an experiment.

second case. Figure 2 shows the time-dependent populations of the wells, where a non-interacting BEC is simulated. The first two cases are analogous to the results of [19]. For the six-mode model we see that the reservoir wells left of the embedded wells are emptying with a slower speed, which was expected, since both wells serve as a common reservoir. The wells to the right are filling analogously. The time that is available for realizing \mathcal{PT} -symmetry is the same for the last two cases, hence the six-mode model gives no advantage with respect to the time that is available. However, there are other advantages discussed in the following.

Of further interest is the time-dependence of the matrix elements, which is shown in Fig. 3. The tunneling elements show almost the same behavior for the cases (ii) and (iii). The difference lies in the onsite energies. Due to the smaller amount of particles per well for the six-mode model the magnitude of the onsite energies is smaller than in case (ii), as well as the rate of change. This could result in an easier experimental realization.

With more wells we now have a second possibility to enlarge the particle reservoir. Besides putting more particles in the two outer wells of the four-mode model we can add more wells. The difference is the resulting onsite energies, which with this method can be brought into an experimentally accessible range.

2. Requiring specific currents

The second possibility for choosing the onsite energies is by requiring specific currents between the additional wells. Of course, the choice of these target currents is free. A somewhat natural choice is to require that each of the reservoir wells should contribute equally to the \mathcal{PT} -symmetric currents. For our six-mode model this means that when wells 3 and 4 are the embedded wells, the current j_{23} is given by the condition (18a), and for j_{12} we require $j_{12} = j_{23}/2$. Similarly we set $j_{56} = j_{45}/2$. The reservoir wells on the left should then be emptying at the same speed, as well as those on the right should fill. The initial conditions and the choice of the onsite energies are then given by the results in Sec. III E. This leads to a scenario that is similar to that of leveling out the onsite energies, the difference is that now we can choose arbitrary initial conditions for the embedded wells and the phases of the reservoir wells can be calculated appropriately, thus extending the possibilities.

When the reservoir wells to the left are emptying at the same speed, this can be unfavorable when one well has a lower initial population than the other: When this well gets empty, the simulation stops although there are particles in the left reservoir. This can be overcome by choosing the specific inter-well currents proportional to the initial population. Suppose that $j_{m-1,m}$ and $j_{m+1,m+2}$ are given by conditions (18). Then we set for the reservoir wells $\dot{n}_k^{\text{tar}} = j_{k-1,m}^{\text{tar}} - j_{k,k+1}^{\text{tar}} \propto n_k(t=0)$. The proportionality constant can be fixed by requiring $j_{m-1,m}$ and $j_{m+1,m+2}$ to fulfill the conditions. In the six-mode model we get for the left reservoir wells

$$j_{12}^{\text{tar}} = -Cn_1(0), \quad j_{12}^{\text{tar}} - j_{23}^{\text{tar}} = Cn_2(0). \quad (50)$$

This can be solved according to

$$j_{12}^{\text{tar}} = -Cn_1(0), \quad j_{23}^{\text{tar}} = -C[n_1(0) + n_2(0)]. \quad (51)$$

For j_{23} we get from condition (18a) $j_{23}^{\text{tar}} = 2\Gamma n_3(0)/\hbar$. The constant C can now be determined and we obtain

$$j_{12}^{\text{tar}} = \frac{2\Gamma n_1(0)n_3(0)}{\hbar[n_1(0) + n_2(0)]}, \quad j_{23}^{\text{tar}} = \frac{2\Gamma n_3(0)}{\hbar}. \quad (52)$$

For an arbitrary number of wells, this can be solved by iteration. The target currents for the right wells are not essential, hence we can choose them to be symmetric to the left wells.

We apply this scenario to a system, where we start with the ground state for $E_k/J_{34} = -5$ for $k = 1, 2, 5, 6$, $E_k = 0$ for $k = 3, 4$, $J_{k,k+1}/J_{34} = 1$ and $g = 1$. In this case, the ground state is normalized to unity, $|\psi|^2 = 1$. We use the adiabatic current ramp with $\Gamma_f/J_{34} = 0.7$ and $t_f = 15\hbar/J_{34}$. The observables and matrix elements are shown in Fig. 4. Clearly, the initial population of wells 1 and 2 are different, however, they get empty at approximately the same time. The target currents obey $j_{12}/j_{23} = j_{56}/j_{45} \approx 0.4589$. With this choice of the

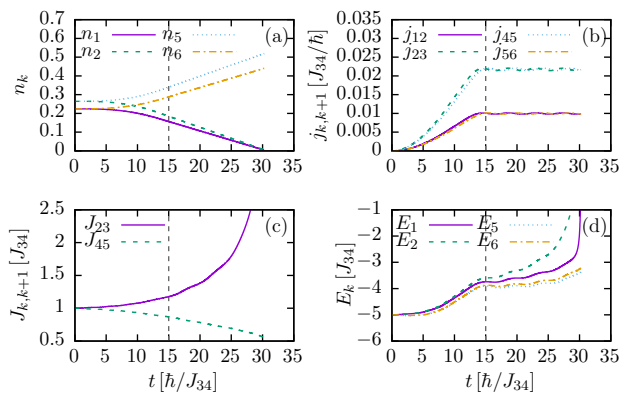


Figure 4. (Color online) Adiabatic current ramp with two reservoir wells on each side with $N_w = 6$ wells. Shown are (a) particle numbers in the reservoir wells, (b) inter-well currents, (c) tunneling elements, and (d) onsite energies. We start with the ground state for the parameters given in the text. The target currents are chosen in such a way that the left reservoir wells get empty at nearly the same time. This allows us to effectively use all particles in the reservoir wells and thus to maximize the time that is available for \mathcal{PT} -symmetry.

currents the onsite energies are no longer approximately equal, so this scenario differs from the previous one. We can now start from arbitrary initial conditions and realize \mathcal{PT} symmetry with more than one reservoir well on each side until all left reservoir wells become empty. Here we give a specific example of an adiabatic current ramp, however, with this choice of target currents we can simulate arbitrary scenarios, that means, starting with a value of $\Gamma \neq 0$ and non-quasi-stationary solutions.

B. More wells

When using more than six wells, as in Sec. IV A, the options are consequently extended. In this section, we give a single example of what can be done.

We realize \mathcal{PT} symmetry using $N_w = 10$ wells and require the currents in such a way that the contribution from each reservoir well is proportional to its initial population. We set $\Gamma/J_{56} = 0.6$, $g/J_{56} = 10$, and start with the ground state for $E_k = 0$ for $k = 5, 6$ and $E_k/J_{56} = -3$ otherwise, furthermore we set for all k $J_{k,k+1}/J_{56} = 1$. Since we start with a finite value of Γ , where the ground state matches to $\Gamma = 0$, this corresponds to a non-quasi-stationary solution. The observables and matrix elements are shown in Fig. 5. The number of particles in the reservoir well on the left of the embedded wells decreases in such a way that the wells get empty at the same time. Thus, the whole reservoir is used. The currents on the left side are proportional to each other, as are those on the right side. The energies on each side are no longer equal, which shows that leveling out the onsite energies does not use the reservoir in an optimal way.

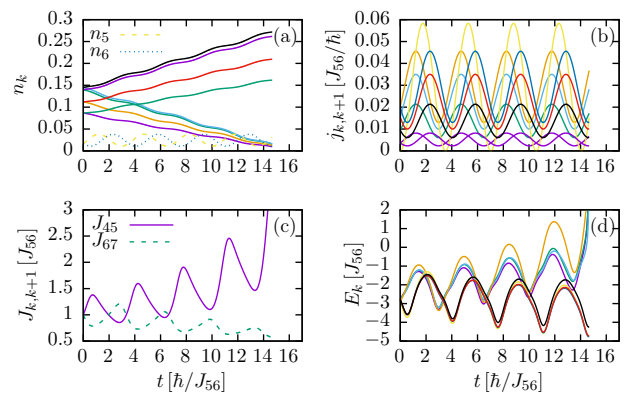


Figure 5. (Color online) Non-quasi-stationary solutions for the parameters $\Gamma/J_{56} = 0.6$ and $g/J_{56} = 10$ with $N_w = 10$ wells. See text for initial conditions. Shown are (a) particle numbers, (b) inter-well currents, (c) tunneling elements, and (d) onsite energies. The currents are chosen such that the reservoir wells are emptying with a rate proportional to the initial population. With this choice the reservoir can be used in an optimal way. Here we give up the leveled out onsite energies.

C. Optical lattices

The use of more and more wells motivates the investigation of the realization of \mathcal{PT} -symmetric BECs in terms of optical lattices, of which the basics are discussed in Sec. III F. Instead of requiring a specific current from each reservoir well, we now simply calculate the energy values of the wells adjacent to the embedded wells and extend the remaining onsite energies such that they build an optical lattice with a linear Stark potential. This idea has been theoretically worked out in Sec. III E.

In our realization, we always consider a *finite* number of wells, as opposed to an infinitely extended optical lattice. Instead of a continuous quantum number q we have a discrete variable, and we must replace the integral in Eq. (42) according to

$$\int_{-\pi}^{\pi} dq \rightarrow \sqrt{\frac{2\pi}{L}} \sum_q, \quad (53)$$

where L is the extension of the finite lattice. The allowed values of q are then $q = 2\pi m/L$ with $m = -(L-1)/2, -(L-1)/2+1, \dots, (L-1)/2$. However, when there is a large number of wells, the use of a continuous quantum number is a valid approximation. We can therefore use the semiclassical approximation discussed in Sec. III F as a description of our system with a time-dependent force $\Delta E(t)$ to manipulate the wave packet. However, a pure Gaussian wave packet cannot describe a \mathcal{PT} -symmetric situation since the population in the embedded wells cannot be constant. Hence, a suitable perturbation of the linear Stark potential must be added.

In Sec. III E we discussed how the energies of the wells adjacent to the embedded wells can be extended to an

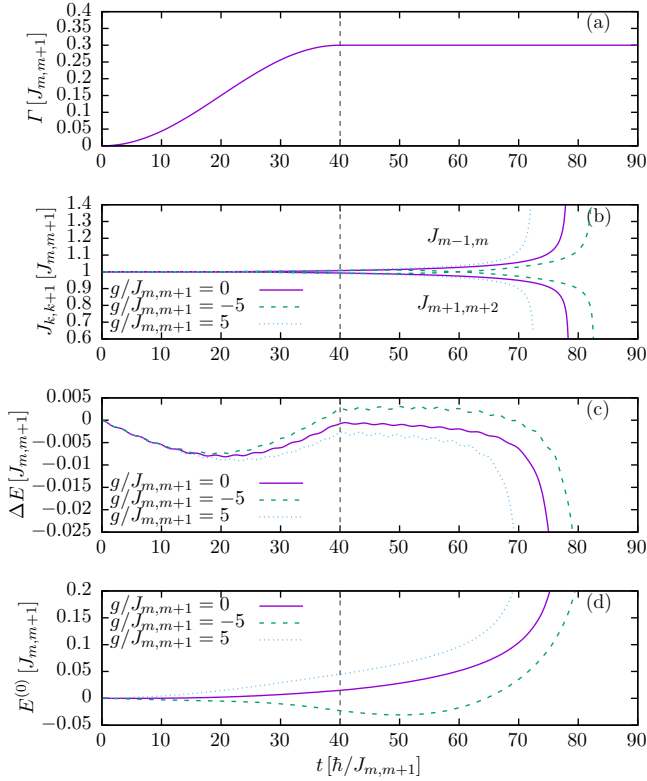


Figure 6. (Color online) (a) \mathcal{PT} parameter Γ , (b) tunneling elements, (c) energy slope ΔE , and (d) energy offset $E^{(0)}$ of the energy distribution (37). For $t = 0$ a Gaussian wave function has been prepared and the \mathcal{PT} symmetry is realized using an adiabatic current ramp for $\Gamma_f/J_{m,m+1} = 0.3$ and $t_f = 40\hbar/J_{m,m+1}$. The calculation is repeated for different values of the interaction strength. For $t < t_f$ the slope ΔE is used to accelerate the wave packet, whereas for $t > t_f$ the slope must be changed to compensate the decrease in population of the moving wave packet. The offset $E^{(0)}$ is the necessary perturbation so that \mathcal{PT} symmetry can be realized.

optical lattice with a linear Stark potential according to Eq. (37) with a slope ΔE of the linear potential and an offset $E^{(0)}$. The offset, where the embedded wells are *not* part of the linear potential, is the perturbation that is necessary to obtain a \mathcal{PT} -symmetric realization as discussed in Sec. III F. With this choice of the onsite energies a realization of \mathcal{PT} symmetry is possible in our developed framework and the formalism of Sec. III F can be used to interpret the results.

For the following simulations we use $N_w = 300$ wells, where the embedded wells are given by $m = 150$ and $m + 1 = 151$, and an adiabatic current ramp with $\Gamma_f/J_{m,m+1} = 0.3$ and $t_f = 40\hbar/J_{m,m+1}$. The starting wave function is given by

$$\psi_n(t=0) = \sqrt[4]{\frac{2(\Delta q)^2}{\pi}} \exp[-(\Delta q)^2(n - n_0(t=0))^2] \quad (54)$$

with the parameters $\Delta q = 0.017$, and $n_0(t=0) = 150.5$

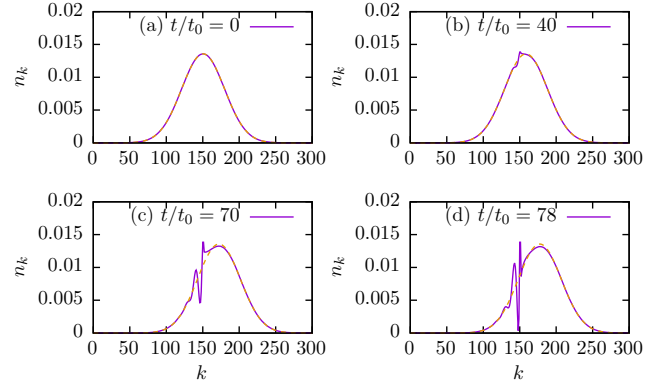


Figure 7. (Color online) Wave function in position space of the scenario of Fig. 6 for different times (a)–(d) and a vanishing interaction strength. The initial Gaussian wave packet is accelerated to the right due to the negative energy slope ΔE . At the same time the purely Gaussian shape is perturbed due to the energy offset. In combination, these effects contribute to the realization of \mathcal{PT} -symmetry in the embedded wells $m = 150$ and $m + 1 = 151$ with a constant number of particles n_{150} and n_{151} . The dashed curves give the wave function of the semiclassical approximation, where the energy offset is ignored.

such that the wave function has no momentum at the beginning and fulfills $n_m = n_{m+1}$. The quantity Δq is chosen so that there are no boundary effects during the simulation time. Figure 6 shows the tunneling elements as well as the parameters ΔE and $E^{(0)}$ for different strengths of interaction. The tunneling elements do not change much over a large range of the simulation time, see Fig. 6(b). Only close to the point, where the realization is no longer possible, the tunneling elements vary noticeably. The time-dependence of the slope ΔE shown in Fig. 6(c) can be explained as follows: At the beginning the \mathcal{PT} -symmetric current is being increased (see Fig. 6(a)) by a negative slope of the linear energy part, and the wave packet is accelerated to the right. At the end of the adiabatic current ramp $t_f = 40\hbar/J_{m,m+1}$, the slope is again close to zero, the acceleration stops and there is a constant current. When the wave packet now moves to the right (as shown in Fig. 7), the population in the reservoir well left of the embedded wells decreases. This is compensated by an increasing negative slope. When coming close to the end of the simulation time, the negative slope must increase and finally diverges to $-\infty$. The influence of the interaction strength can be understood by noticing that a repulsive interaction leads to a faster dispersion of the wave packet and hence a slightly larger negative slope is necessary. The opposite is true for an attractive interaction, for some time interval the slope even can get positive. The energy offset $E^{(0)}$ is zero at the beginning, and then must change to maintain \mathcal{PT} symmetry. The more distant the center of the wave packet has moved, the more the offset must vary, which finally leads to a divergence of $E^{(0)} \rightarrow \infty$.

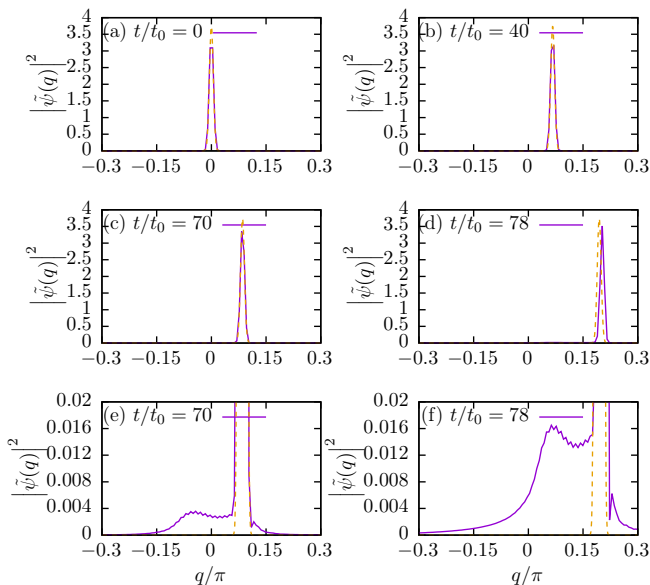


Figure 8. (Color online) Same as Fig. 7, but for the wave function in momentum space. The dashed line gives the wave function of the semiclassical approximation. The last row (e)–(f) shows an enlarged plot of the previous row (c)–(d). In momentum space, the wave function is dominated by the sharp peak in q_0 , of which the time-dependence can be calculated according to the semiclassical approximation and which gives a good description for the dominating peak. Only in the enlarged views (e)–(f) one notices the perturbation due to the energy offset. This perturbation is getting stronger during the simulation time, however, it does not reach the magnitude of the momentum peak.

Figure 7 shows the population per well for different times. The initial Gaussian wave packet in Fig. 7(a) is soon disturbed by the energy offset $E^{(0)}$. Close to the left of the embedded wells is a dip in the population which further decreases during the simulation. The wave function is highly perturbed close to the embedded wells, however, for the wells far away the wave packet is well described by the semiclassical approximation. Close to the time when the simulation breaks down particles are still left in the reservoir wells. We conclude that with the energy distribution according to Eq. (37) the particles in the reservoir cannot be completely used, which is the cost of this simple energy distribution.

Of further interest is the Fourier transform of the wave function that can be calculated according to

$$\tilde{\psi}(q) = \frac{1}{2\pi} \sum_k \exp(-iqk) \psi_k. \quad (55)$$

Figure 8 shows this Fourier transform for a selection of different times. As to be expected, it is dominated by a sharp peak in q -space. This dominance does not vanish during simulation time and can be reasonably described by the semiclassical approximation. The position of this peak moves according to Eq. (46). The energy offset induces a perturbation, which is in particular visible near

the end of the simulation time $t \gtrsim 70\hbar/J_{m,m+1}$. Note that its maximum magnitude is smaller than one percent of the momentum peak.

V. CONCLUSION AND OUTLOOK

We have developed the basic idea to realize a \mathcal{PT} -symmetric two-mode model by embedding this system into a larger Hermitian system with in total at least four wells where the additional wells are considered as reservoir wells. In the limit of large number of wells \mathcal{PT} symmetry is realized by a tilted optical lattice where the embedded double well is a necessary defect. The coupling of the embedded wells to the reservoir wells is due to the overlapping wave functions between adjacent wells. It has already been shown that the necessary potential can be created experimentally [22]. The coupling of overlapping wave functions is experimentally accessible contrary to the methods used in [20, 21], where a coupling is assumed without giving possible realizations of such a coupling and thus leaving some ambiguity. With our method we are thus able to give a realistic scenario for realizing \mathcal{PT} symmetry where all parameters used in a possible experiment are determined.

For the theoretical investigations we used the matrix model developed in [19], where we concentrated on using the four-mode model. We applied all the theoretical results to calculate the dynamical evolution of the realizations of \mathcal{PT} symmetry. Due to a finite particle reservoir the time that is available for realizing \mathcal{PT} symmetry is always limited. For a four-well system this time can be extended by filling more particles in the reservoir wells. However, a large difference between the number of particles in the embedded wells on one hand and the particle population in the embedded wells on the other hand can be a huge experimental challenge for both preparing such a state and measuring the particle numbers. Furthermore, such a large difference can make the necessary matrix elements of the Hamiltonian (6) extraordinarily large. For these reasons, we extended the model to more than two reservoir wells in this article, such that there are more possible realizations with an arbitrary number of reservoir wells. Thus, we have a wealth of possible realization of \mathcal{PT} symmetry, and an experimentalist can choose the system parameters such that they are in an accessible range. We analyzed a system with a large number of wells in the framework of optical lattices. In that sense, \mathcal{PT} symmetry can be interpreted by a moving and accelerating wave packet that scatters at a defect of a tilted optical lattice, which leads to a realization of \mathcal{PT} symmetry at that double well.

Many of the investigations of \mathcal{PT} -symmetric BECs were performed in terms of the mean-field approximation. First extensions were made [28], and it could be possible to study a realization using the many-particle Bose-Hubbard model. The results from the matrix model in this work could then be used as a possible road map.

Due to the higher degrees of internal freedom a comparison with the results obtained from the many-particle quantum master equation would be of special interest.

Land Baden-Württemberg.

ACKNOWLEDGMENTS

This work was supported by DFG. M.K. is grateful for support from the Landesgraduiertenförderung of the

-
- [1] C. M. Bender and S. Boettcher, Phys. Rev. Lett. **80**, 5243 (1998).
 - [2] A. Ruschhaupt, F. Delgado, and J. G. Muga, J. Phys. A **38**, 171 (2005).
 - [3] S. Klaiman, U. Günther, and N. Moiseyev, Phys. Rev. Lett. **101**, 080402 (2008).
 - [4] A. Guo, G. J. Salamo, D. Duchesne, R. Morandotti, M. Volatier-Ravat, V. Aimez, G. A. Siviloglou, and D. N. Christodoulides, Phys. Rev. Lett. **103**, 093902 (2009).
 - [5] C. E. Rüter, K. G. Makris, R. El-Ganainy, D. N. Christodoulides, M. Segev, and D. Kip, Nat. Phys. **6**, 192 (2010).
 - [6] Y. D. Chong, L. Ge, and A. D. Stone, Phys. Rev. Lett. **106**, 093902 (2011).
 - [7] L. Ge, Y. D. Chong, S. Rotter, H. E. Türeci, and A. D. Stone, Phys. Rev. A **84**, 023820 (2011).
 - [8] M. Liertzer, L. Ge, A. Cerjan, A. D. Stone, H. E. Türeci, and S. Rotter, Phys. Rev. Lett. **108**, 173901 (2012).
 - [9] J. Schindler, A. Li, M. C. Zheng, F. M. Ellis, and T. Kottos, Phys. Rev. A **84**, 040101 (2011).
 - [10] H. Ramezani, J. Schindler, F. M. Ellis, U. Günther, and T. Kottos, Phys. Rev. A **85**, 062122 (2012).
 - [11] J. Schindler, Z. Lin, J. M. Lee, H. Ramezani, F. M. Ellis, and T. Kottos, J. Phys. A **45**, 444029 (2012).
 - [12] S. Bittner, B. Dietz, U. Günther, H. L. Harney, M. Miskioğlu, A. Richter, and F. Schäfer, Phys. Rev. Lett. **108**, 024101 (2012).
 - [13] E. M. Graefe, H. J. Korsch, and A. E. Niederle, Phys. Rev. Lett. **101**, 150408 (2008).
 - [14] E. M. Graefe, U. Günther, H. J. Korsch, and A. E. Niederle, J. Phys. A **41**, 255206 (2008).
 - [15] E.-M. Graefe, H. J. Korsch, and A. E. Niederle, Phys. Rev. A **82**, 013629 (2010).
 - [16] H. Cartarius and G. Wunner, Phys. Rev. A **86**, 013612 (2012).
 - [17] D. Haag, D. Dast, A. Löhle, H. Cartarius, J. Main, and G. Wunner, Phys. Rev. A **89**, 023601 (2014).
 - [18] D. Dast, D. Haag, H. Cartarius, J. Main, and G. Wunner, J. Phys. A **46**, 375301 (2013).
 - [19] M. Kreibich, J. Main, H. Cartarius, and G. Wunner, Phys. Rev. A **90**, 033630 (2014).
 - [20] F. Single, H. Cartarius, G. Wunner, and J. Main, Phys. Rev. A **90**, 042123 (2014).
 - [21] R. Gutöhrlein, J. Schnabel, I. Iskandarov, H. Cartarius, J. Main, and G. Wunner, J. Phys. A **48**, 335302 (2015).
 - [22] K. Henderson, C. Ryu, C. MacCormick, and M. G. Boshier, New J. Phys. **11**, 043030 (2009).
 - [23] P.-O. Löwdin, J. Chem. Phys. **18**, 365 (1950).
 - [24] E.-M. Graefe, J. Phys. A **45**, 444015 (2012).
 - [25] M. Kreibich, J. Main, H. Cartarius, and G. Wunner, Phys. Rev. A **87**, 051601(R) (2013).
 - [26] O. Morsch and M. Oberthaler, Rev. Mod. Phys. **78**, 179 (2006).
 - [27] M. Kreibich, *Realizations of PT-symmetric Bose-Einstein condensates with time-dependent Hermitian potentials*, Ph.D. thesis, Universität Stuttgart (2015).
 - [28] D. Dast, D. Haag, H. Cartarius, and G. Wunner, Phys. Rev. A **90**, 052120 (2014).